Annals of the Academy of Romanian Scientists
Series on Physics and Chemistry Sciences
ISSN 2559 – 1061 Volume 5, Number 1/2020

ALPHA-RESONANCES IN MEDIUM AND HEAVY NUCLEI I. Review of phenomenological models

D.S. Delion*, A. Dumitrescu†, and V.V. Baran‡

Abstract

The low-lying rotational bands in light nuclei were explained a long time ago by α-clusters orbiting around the remaining core. These quasimolecular states are related to an enhancement of the elastic α-particle cross section at large angles, the so-called Anomalous Large Angle Scattering (ALAS) phenomenon. On the other hand, α-particles were evidenced by the discovery of the α-decay for nuclei with $Z > 50$. We used a phenomenological model of an α-particle moving in a pocket-like potential, able to explain the ALAS phenomenon, in order to understand the main features of the decay data between ground and excited states. Then we extended the Brink model, explaining giant resonances, and presented a possibility to detect α-like collective resonances.

keywords: alpha decay, resonant state, decay width

https://doi.org/10.56082/annalsarsciphyschem.2020.1.38

*delion@theory.nipne.ro [1] Horia Hulubei National Institute for Physics and Nuclear Engineering, Reactorului 30, P.O. Box MG-6, RO-077125, Bucharest-Măgurele, România; [2] Academy of Romanian Scientists, 3 Ilfov RO-050044, Bucharest, România; [3] Bioterra University, 81 Gârlei RO-013724, Bucharest, România; Acknowledgment for financial support: Grant of the Romanian Ministry of Research and Innovation, CNCS - UEFISCDI, PN-19060101/2019-2022;

†[1] Horia Hulubei National Institute for R&D in Physics and Nuclear Engineering, Str. Reactorului no. 30, P.O. Box MG-6, RO-077125, Bucharest-Măgurele, România;

‡[1] Horia Hulubei National Institute for R&D in Physics and Nuclear Engineering, Str. Reactorului no. 30, P.O. Box MG-6, RO-077125, Bucharest-Măgurele, România; [4] Department of Physics, University of Bucharest, 405 Atomiştilor, POB MG-11, RO-077125, Bucharest-Măgurele, România;

1 Introduction

α-clusters can be evidenced as building blocks in nuclei, due to the large α-particle binding energy [1, 2, 3, 4]. Let us first of all mention the pair staggering shape of binding energies along the so-called α-lines, defined by adding $N_\alpha = A/[2(N + Z)]$ quartets on top of a double magic nucleus plus a given number of neutron pairs [5]. This behaviour is similar to the well-known even-odd staggering along isotope/isotone chains, induced by the pairing interaction, and lead to the concept of the isospin pairing between proton and neutron pairs [6]. The α-like structures can directly be probed in the ground states of light nuclei with a quarted structure like ^{8}Be, ^{12}C, ^{16}O, ... ^{40}Ca [7]. On the other hand, clustering is favored at smaller nuclear densities [8], as it is the case in some excited 0^+ states, called Hoyle states with a very pronounced quartet structure [9].

Clustering structures were also evidenced by the α-like rotational bands in light nuclei, seen as resonant structures in the elastic cross section of the α-particle scattering on light nuclei. These structures, called quasimolecular states [10], are usually connected to the so-called Anomalous Large Angle Scattering (ALAS), seen as an enhancement of the ratio between the angular distribution and Rutherford distribution at large angles.

The α-particles were first of all evidenced by the α-decay mode for nuclei with $Z \geq 50$. It turns out that this process can be understood in terms of a pocket-like α-core interaction, similar to the quasimolecular description in light nuclei. The aim of this paper is to review the phenomenological approaches concerning the α-like resonances in α-decaying nuclei.

2 Resonant description of the α-decay

The dynamics of an α-daughter system emitted from a parent nucleus

$$P \rightarrow D + \alpha \ , \tag{2.1}$$

is described by the time-dependent Schrödinger equation

$$\widehat{H}\Phi(\mathbf{R},t) \equiv \left[-\frac{\hbar^2\nabla_R^2}{2\mu} + V(\mathbf{R})\right]\Phi(\mathbf{R},t) = i\hbar\frac{\partial\Phi(\mathbf{R},t)}{\partial t} \ , \tag{2.2}$$

where μ is the reduced mass of the α-core system. The general time-dependent solution

$$\Phi(\mathbf{R},t) = \Psi(\mathbf{R})e^{-iEt/\hbar} \ , \tag{2.3}$$

depends on a complex energy

$$E = Q - i\frac{\Gamma}{2} \ , \tag{2.4}$$

where the real part denotes the Q-value of the process. The wave function describing a decay process should be proportional with an outgoing wave at large distances

$$\Psi(\mathbf{R}) \to_{R\to\infty} \mathcal{N}\frac{e^{i\kappa R}}{R} \ , \tag{2.5}$$

where $\mathcal{N}$ is called scattering amplitude and κ denotes the asymptotic wave number, defined by the usual relations

$$Q = \frac{p^2}{2\mu} \ , \quad p = \hbar\kappa \ , \tag{2.6}$$

Thus, the incoming wave is missing and therefore the S-matrix of the process, proportional to the ratio between outgoing and ingoing waves, has a pole corresponding to this energy. By using the continuity equation, one obtains the probability flux being proportional to the imaginary part of the energy

$$\Gamma = \hbar v|\mathcal{N}|^2 \ , \quad v = p/\mu \ , \tag{2.7}$$

provided the normalisation condition in the internal region is fulfilled

$$\int |\Psi(\mathbf{R})|^2 d\mathbf{R} = 1 \ . \tag{2.8}$$

Let us mention here that the half life is defined by the standard relation

$$T_{1/2} = \frac{\hbar \ln 2}{\Gamma} \ . \tag{2.9}$$

For all measured α-decays the Coulomb barrier $V_B = V(R_B)$ surounding the nuclear α-core interaction is large enough ($V_B > 2Q$), leading to the following estimate

$$\frac{\Gamma}{Q} < 10^{-10} \ . \tag{2.10}$$

Thus, the stationary condition can be considered as a very good approximation and the radial wave function, satisfying the equation

$$\widehat{H}\Psi(\mathbf{R}) = E\Psi(\mathbf{R}) \ , \tag{2.11}$$

decreases inside the barrier by many orders of magnitude, being very close to a bound state. Therefore the integration in the normalisation condition (2.8) can be performed only until the external tourning point. Let us mention in this context that the radial solution can be expanded in multipoles

$$\Psi_m(\mathbf{R}) = \sum_l \frac{f_l(R)}{R} Y_{lm}(\widehat{R}) \ , \tag{2.12}$$

and at large distances, where the interaction becomes spherical and purely Coulombian, the equation (2.11) can be written

$$\left[-\frac{d^2}{d\rho^2}+\frac{l(l+1)}{\rho^2}+\frac{\chi}{\rho}-1\right]f_l(r)=0\ , \tag{2.13}$$

in terms of the reduced radius and Coulomb parameter respectively

$$\begin{aligned}\rho &= \kappa R \\ \chi &= \frac{4Z_De^2}{\hbar v}\ ,\end{aligned} \tag{2.14}$$

where Z_D is the charge of the daughter nucleus. If the interaction potential $V(\mathbf{R})$ is defined for all radii, the normalised wave function in the internal region with the outgoing boundary condition (2.5) is found for few discrete values $Q_k \leq V_B$. They are called α-like, or Gamow resonances and at large distances are proportional to the outgoing solutions of Eq. (2.13) called Coulomb-Hankel waves

$$f_l(R)\rightarrow_{R\rightarrow\infty}\mathcal{N}_l H_l^{(+)}(\rho,\chi)=\mathcal{N}_l\left[G_l(\rho,\chi)+F_l(\rho,\chi)\right]\ , \tag{2.15}$$

written in terms of irregular (regular) Coulomb waves G_l (F_l). The lowest eigenstate with $k=1$ describes the α-decay process connecting ground states of parent and daughter nuclei with the eigenvalue equal to the experimental Q-value. This can be achieved by changing the depth of the α-core nuclear interaction. We will show later that it is possible to find in this way the first and second α-like resonances fulfilling the under-barrier condition $Q_k \leq V_B$. It is important to point out that the internal shape of the nuclear part can in principle determine the position of the second resonant state, which can experimentally be detected as a maximum in the excitation function of α-scattering cross sections close to the Coulomb barrier. We will analyse this possibility in a special Section.

By using the expansion of the wave function (2.12), the total decay width becomes a sum of partial components

$$\Gamma=\sum_l \hbar v|\mathcal{N}_l|^2\equiv\sum_l\Gamma_l\ . \tag{2.16}$$

The matching condition (2.15) between each internal component and the corresponding Coulomb wave at some radius R inside the pure Coulomb barrier leads to the following factorisation

$$\Gamma_l=P_l(R)\gamma_l^2\ (R)\ , \tag{2.17}$$

in terms of the penetrability and reduced width

$$\begin{aligned}P_l(R) &= \frac{2\rho}{\left|H_l^{(+)}(\rho,\chi)\right|^2}\approx\frac{2\rho}{G_l^2(\rho,\chi)} \\ \gamma_l^2(R) &= \frac{\hbar^2 f_l^2(R)}{2\mu R}\ .\end{aligned} \tag{2.18}$$

The theoretical decay width (2.16) is obviously different from its experimental value. The ratio

$$S_\alpha = \frac{\Gamma_{exp}}{\Gamma_{th}} \ , \tag{2.19}$$

defines the α-decay spectroscopic factor. Let us stress here that this phenomenological approach using the above mentioned normalisation condition of the wave function determined by an α-core potential cannot determine this physical quantity. Only a microscopic approach, describing the α-formation probability, is in principle able to perform this task.

3 α-daughter interaction

The realistic α-daughter interaction can be estimated in terms of the double folding between the nuclear densities [11, 12, 13], i.e.

$$V(\mathbf{R},\Omega) = \int d\mathbf{r}_D \int d\mathbf{r}_\alpha \rho_D(\mathbf{r}_D)\rho_\alpha(\mathbf{r}_\alpha) v(\mathbf{R}+\mathbf{r}_D-\mathbf{r}_\alpha) \ , \tag{3.1}$$

where $\mathbf{R}$ is the α-core radius, Ω are the Euler angles with respect to the symmetry axis of the daughter nucleus and v denotes the nucleon-nucleon force, usually taken as the M3Y potential [12]. This procedure was widely used to compute the potential between heavy ions by using for their densities a Woods-Saxon shape. In our case the density of the daughter nucleus is given by such a distribution, while that of the α-particle by a Gaussian with standard parameters [14].

The potential (3.1) can be divided into a spherical and a deformed component

$$V(\mathbf{R},\Omega) = V_0(R) + V_d(\mathbf{R},\Omega) \ . \tag{3.2}$$

By expanding the nuclear densities in multipoles one obtains the deformed part of the interaction

$$V_d(\mathbf{R},\Omega) = \sum_{\lambda>0} V_\lambda(R)\mathcal{Y}_\lambda(\widehat{R},\Omega) \ . \tag{3.3}$$

Here the angular part of the wave function has the following ansatz

$$\mathcal{Y}_\lambda(\widehat{R},\Omega) = \Big[Y_\lambda(\widehat{R}) \otimes Y_\lambda(\Omega)\Big]_0 \ . \tag{3.4}$$

Due to the Pauli principle, the α-particle can exist only on the nuclear surface, where the nuclear density becomes less than 20% of the standard saturation value at equilibrium. Therefore, the local potential simulating this situation should have a pocket-like molecular shape centered on the nuclear surface, In Fig. 1 we plotted the spherical potential corresponding to the decay $^{212}Po \rightarrow ^{208}\ Pb + \alpha$ by a solid

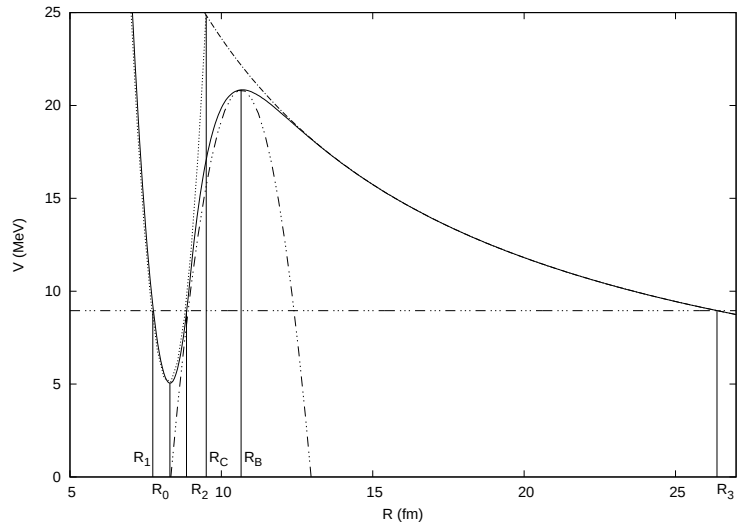

Figure 1: Realistic alpha-daughter double-folding plus ho repulsive potential given by a solid line for the system $^{208}Pb + \alpha$ versus radius. The repulsive harmonic oscillator part is plotted by dots, the parabolic approximation of the realistic nuclear attraction estimated by the double folding procedure by triple-dot dashes and the pure Coulomb potential by a dot-dashed line. The horizontal line corresponds do the Q-value of the emission process $^{212}Po \rightarrow^{208} Pb + \alpha$.

curve. The internal repulsion, given by the dotted ho potential, simulates the Pauli principle forbiding the existence of the α-particle inside the nucleus. The horizontal line denotes the energy release (Q-value). Let us mention that the three solutions of the equation $V(R) = Q$ are called turning points: $R_1,\ R_2,\ R_3$. Notice that the ho repulsion is matched to the realistic attractive part at the second turning point R_2.

4 Universal rule for the reduced width

Let us consider a schematic α-daughter interaction given by the ho potential, plotted by dots in Fig. 1, matched to a pure Coulomb repusion at R_C. By considering the Q-value as the first resonant eigenstate in the shifted ho well $Q - V(R_0) = \frac{1}{2}\hbar\omega$, together with the continuity condition at the top of the barrier R_C, one obtains the following relation

$$\hbar\omega_0 \frac{\beta_0 (R_C - R_0)^2}{2} = V_{frag}(R_C) + \frac{1}{2}\hbar\omega_0 \ , \tag{4.1}$$

where we introduced the so called fragmentation (or driving) potential

$$V_{frag}(R_C) = V_C(R_C) - Q \ . \tag{4.2}$$

For a shifted ho well one has for the ground state

$$f_{int}(R) = A_0^2 e^{-\beta_0 (R-R_0)^2/2} \ . \tag{4.3}$$

By using Eq. (4.1) one obtains the following relation

$$\log_{10} \gamma^2(R_C) = \log_{10} \left[\frac{\hbar^2}{2\mu R_C} f_{int}^2(R_C) \right] = -\frac{log_{10} e^2}{\hbar\omega_0} V_{frag}(R_C) + \log_{10} \frac{\hbar^2 A_0^2}{2e\mu R_C} \ , \tag{4.4}$$

called the universal rule for the reduced width [15]. Let us mention that it does not depend upon the equilibrium radius R_0 and the ho frequency of the internal potential $\hbar\omega_0$ can be considered as a free parameter, together with the matching radius R_C.

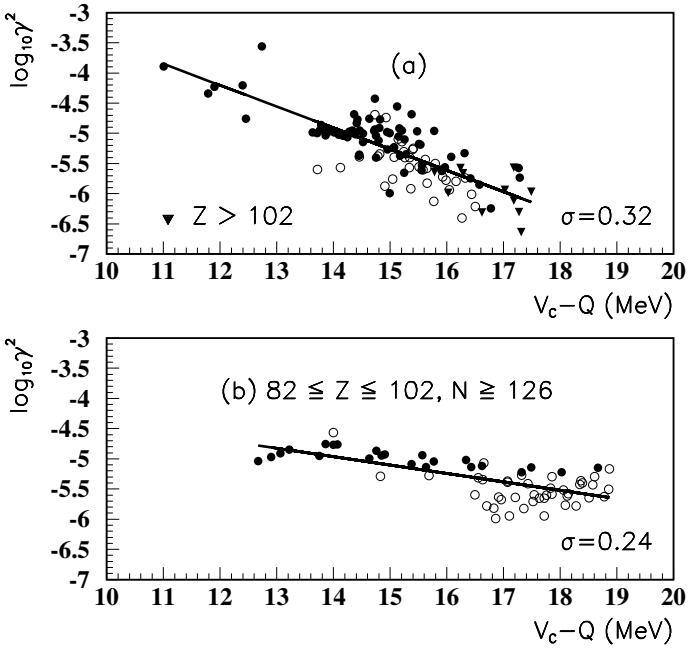

Figure 2: Logarithm of the reduced α-decay width for even-even emitters versus the fragmentation potential $V_{frag} = V_C(R_C) - Q$, for $R_C = 1.2(A_D^{1/3} + 4^{1/3})$. By open symbols are given emitters above ^{208}Pb and by dark symbols all other emitters.

In Fig. 2 we plotted the logarithm of the reduced width estimated at the geometrical touching radius

$$R_C = 1.2(A_D^{1/3} + 4^{1/3}) \tag{4.5}$$

by considering in panel (b) even-even emitters with $82 \leq Z \leq 102,\ N \geq 126$ and in panel (a) all other cases. By open symbols are given emitters above ^{208}Pb and by dark symbols all other emitters. One clearly sees that the slope is indeed negative, as predicted by the universal law (4.4). This is clear evidence of the α-clustering on the nuclear surface, seen as an α-like resonace in a pocket-like potential.

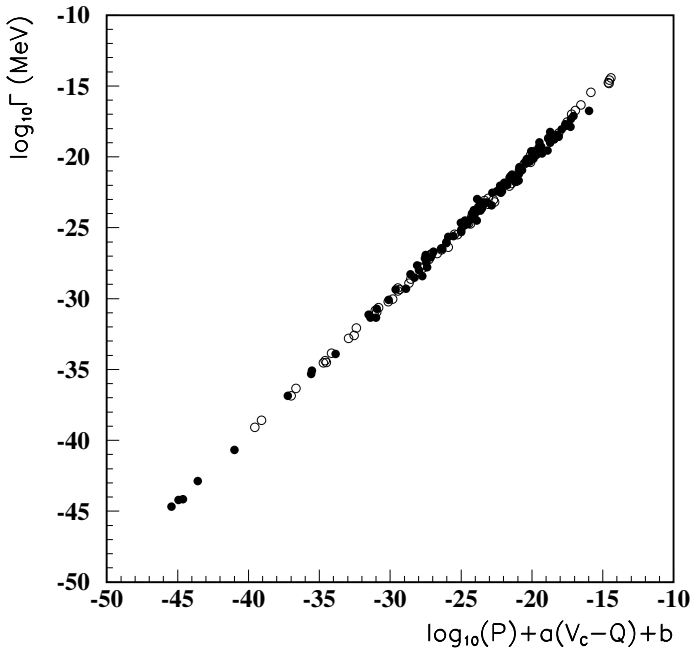

Figure 3: Logarithm of the α-decay width for even-even emitters versus the fragmentation potential $\log P + aV_{frag} + b$. The symbols are the same as in Fig. 2.

In Fig. 3 we plotted the logarithm of the decay width versus $\log_{10} P + aV_{frag} + b$, where we considered different fitting parameters for the two panels in Fig. 2, namely

(a): $a_1 = -0.353,\ b_1 = +0.028,\ \hbar\omega_0 = 17.014\ MeV$;

(b): $a_2 = -0.139,\ b_2 = -3.013,\ \hbar\omega_0 = 43.055\ MeV$.

This plot expains the well known universal Viola-Seaborg dependence [16] versus the variable $V \equiv (c_1 Z_D + c_2)Q^{-1/2} + c_3 Z_D + c_4$, due to the fact that $\log_{10} P \sim (c_1 Z_D + c_2)Q^{-1/2}$ and $V_{frag} \sim Z_D$.

Let us finally mention that this universal law for the reduced width is also valid for proton and heavy cluster emission [15].

5 Coupled channels approach for α-like resonances

For the emission process connecting some states

$$P(J_P) \to D(J) + \alpha(L), \tag{5.1}$$

the wave function describing the α-daughter dynamics can be expanded as follows

$$\Psi^{(P)}_{J_P M_P}(\mathbf{R}) = \sum_{c=1}^{N} \frac{\psi_c(R)}{R} \mathcal{Y}_c(\Omega, \widehat{R}), \tag{5.2}$$

where $c = (J, L, J_P)$ is the channel index and the core-angular harmonics, depending on the daughter coordinates Ω and α-particle angles $\widehat{R}$, are defined by [17]

$$\mathcal{Y}_c(\Omega, \widehat{R}) = \left[\Psi^{(D)}_J(\Omega) \otimes Y_L(\widehat{R})\right]_{J_P M_P}. \tag{5.3}$$

For α-decays from the ground states (gs) of even-even nuclei with $J_P = 0^+$, one has $c = J = L$=even

$$\mathcal{Y}_L(\Omega, \widehat{R}) = \left[\Psi^{(D)}_L(\Omega) \otimes Y_L(\widehat{R})\right]_0. \tag{5.4}$$

In the case of rotational nuclei we have $\Psi^{(D)}_{LM}(\Omega) = Y_{LM}(\Omega)$, and the final state corresponds to a "quasimolecular state" in which the daughter nucleus and α-particle rotate in opposite directions with total momentum $J_P = 0$. For vibrational nuclei, $\Psi^{(D)}_{LM}$ is a vibrational wave function and the picture corresponds to a "quasimolecule" where the two partners vibrate in opposite directions.

For transitions from odd-mass nuclei, J_P and J have half-integer values and the α-particles are emitted with angular momenta $|J_P - J| \le L \le J_P + J$. The resonant states have positive parity for L=even and negative parity for L=odd. The daughter wave function has a core-quasiparticle ansatz

$$\Psi^{(D)}_{JM}(\Omega, \mathbf{r}) = \sum_{Ij} X^J_{Ij} \left[\Phi_I(\Omega) \otimes \phi_j(\mathbf{r})\right]_{JM}, \tag{5.5}$$

where the coefficients are found by diagonalizing a core-quasiparticle interaction reproducing the energy spectrum. Notice that a rotational band with $J \ge j$ is defined by considering only a given quasiparticle orbital j in the above superposition.

Let us mention that the Coherent State Model (CSM) description describes the two limits in a unified way by changing a "deformation parameter" d, which enters the coherent superposition of quadrupole bosons $\exp(db^\dagger_{2K})$ [18, 19].

The α-daughter dynamics is described by the stationary Schrödinger equation

$$H\Psi_{J_P M_P}(\Omega, \mathbf{R}) = Q\Psi_{J_P M_P}(\Omega, \mathbf{R}). \tag{5.6}$$

An α-decaying state is identified with a narrow resonant solution that contains only outgoing components, called Gamow resonances. The Hamiltonian

$$H = -\frac{\hbar^2}{2\mu}\nabla_R^2 + H_D(\Omega) + V_0(\Omega, R) + V_d(\Omega, \mathbf{R}) \tag{5.7}$$

contains the kinetic term, a term describing the dynamics of the nuclear core $H_D(\Omega)$

$$H_D \Psi^{(D)}_{JM_J}(\Omega) = E_c \Psi^{(D)}_{JM_J}(\Omega), \tag{5.8}$$

and the α-core potential, which we split into spherical and deformed parts. By using the orthonormality of the core-angular harmonics in the superposition (5.2), one obtains the system of differential equations for radial components [17]

$$\frac{d^2\psi_c(R)}{d\rho_c^2} = \sum_{c'=1}^{N} A_{cc'}(R)\psi_{c'}(R),\ c = 1, ..., N\ , \tag{5.9}$$

where the matrix

$$A_{cc'}(R) \ = \ \left[\frac{L_c(L_c+1)}{\rho_c^2} + \frac{V_0(\Omega, R)}{Q_\alpha - E_c} - 1\right]\delta_{cc'} + \frac{\langle \mathcal{Y}^{(c)}_{J_P} | V_d(\Omega, \mathbf{R}) | \mathcal{Y}^{(c')}_{J_P} \rangle}{Q_\alpha - E_c}, \tag{5.10}$$

is given in terms of the channel reduced radius

$$\rho_c \ = \ \kappa_c R, \quad \kappa_c = \sqrt{\frac{2\mu(Q_\alpha - E_c)}{\hbar^2}}. \tag{5.11}$$

Let us mention that at large distances the potential becomes spherical ($V_d \to 0$) and purely Coulombian. The external solutions in each channel c can be found by superposition

$$\psi_c^{(ext)}(R) \ = \ \sum_{a=1}^{N} \mathcal{H}^{(+)}_{ca}(R)\mathcal{N}_a. \tag{5.12}$$

Here we have involved the columns of the fundamental matrix of Coulomb solutions with outgoing Coulomb-Hankel asymptotics

$$\begin{aligned} \mathcal{H}^{(+)}_{ca}(R) \ &= \ \mathcal{G}_{ca}(R) + i\mathcal{F}_{ca}(R) \xrightarrow[R\to\infty]{} \delta_{ca} H^{(+)}_{L_c}(R) \\ &= \ \delta_{ca}\left[G_{L_c}(R) + iF_{L_c}(R)\right], \end{aligned} \tag{5.13}$$

where c denotes the channel and a the resonant eigenvalue index. Inside the Coulomb barrier, it coincides with the real matrix of irregular Coulomb solutions $|\mathcal{H}^{(+)}_{ca}(R)| \approx \mathcal{G}_{ca}(R)$. The unknown coefficients $\mathcal{N}_a$ are called scattering amplitudes.

¿From the continuity equation one obtains the total decay width as a sum of partial widths [17]

$$\begin{aligned}\Gamma &= \sum_c \Gamma_c = \sum_c \hbar v_c \lim_{R\to\infty} |f_c(R)|^2 \\ &= \sum_c \hbar v_c |\mathcal{N}_c|^2, \end{aligned} \tag{5.14}$$

depending on scattering amplitudes and asymptotic velocities $v_c = \kappa_c/\mu$. By inverting Eq. (5.12) and using (7.21), the external components of the wave function at some point R inside the α-daughter potential can be expressed

$$\psi_c^{(ext)}(R) = \sum_{a=1}^{N} \mathcal{H}_{ca}^{(+)}(R)\sqrt{\frac{\Gamma_a}{\hbar v_a}},\ c = 1, ..., N, \tag{5.15}$$

in terms of the partial decay widths Γ_a and asymptotic channel velocities.

Let us mention that for the spherical one-channel limit with L_c=0, by considering the matching condition $\psi^{(int)}(R) = \psi^{(ext)}(R)$, Eq. (5.15) becomes the well known relation

$$\Gamma_0 = \hbar v_0 \left[\frac{\psi_0^{(int)}(R)}{\mathcal{G}_{00}(R)}\right]^2. \tag{5.16}$$

6 Systematics of α-clusters on the nuclear surface

Microscopic calculations within the mean field plus pairing approach evidenced that the α-formation amplitude has a shifted gaussian shape centered on the nuclear surface [17], mainly concentrated in the monopole component. This conclusion is also supported by a systematic analysis of particle and heavy cluster emission processes [15]. The coupled channels analysis confirmed a similar behavior of resonant solutions [19]

$$\psi_0^{(int)}(X) = A_0\sqrt{\frac{1}{N}}\sqrt{\frac{\beta_0}{\pi}}e^{-\beta_0 X^2/2}\ , \tag{6.1}$$

where $X = R - R_0$ is the shifted radial coordinate and N the number of channels. Here, A_0 denotes the cluster amplitude and β_0 the ho parameter of the monopole component

$$\begin{aligned}\beta_0 &= \frac{1}{b_0^2} = \frac{m_\alpha \omega_0}{\hbar} = f\hbar\omega_0, \\ f &\equiv \frac{m_\alpha c^2}{(\hbar c)^2} \sim 0.096\ (\mathrm{MeV}^{-1}\ \mathrm{fm}^{-2}), \end{aligned} \tag{6.2}$$

which can be written in terms of the ho length parameter b_0. We considered that for heavy nuclei one has $\mu \approx m_\alpha$. This wave function is generated by a shifted ho α-daughter local potential

$$V_0^{(int)}(X) = v_0 + \frac{1}{2}\hbar\omega_0\beta_0 X^2. \tag{6.3}$$

We matched this potential to a realistic external interaction, given by the double folding α-nucleus potential in terms of the M3Y nucleon-nucleon plus Coulomb proton-proton interaction [19]. The parameters were determined by α-scattering experiments. For the α-particle, we assumed a gaussian distribution with b_α=1.19 fm [11, 12].

We match the internal shifted ho potential to the monopole component of the external double folding potential $V_0(R)$. The same remains valid for the wave function. The unknown coefficients v_0, β_0 and R_0, are determined by using the following matching relations

$$\begin{aligned} v_0 + \frac{1}{2f}\beta_0^2 X_m^2 &= V_0(R_m)\ , \quad X_m = R_m - R_0 \\ \frac{1}{f}\beta_0^2 X_m &= V_0'(R_m) \\ \ln'\psi_0^{(int)}(X_m) &= -\beta_0 X_m = \ln'\psi_0^{(ext)}(R_m). \end{aligned} \tag{6.4}$$

The Q-value is given by experimental data and therefore one obtains the ho parameter and X_m from the last two equations

$$\begin{aligned} \beta_0 &= -\frac{fV_0'(R_m)}{\ln'\psi_0^{(ext)}(R_m)} \\ &= -\frac{\ln'\psi_0^{(ext)}(R_m)}{X_m} = \sqrt{\frac{fV_0'(R_m)}{X_m}}. \end{aligned} \tag{6.5}$$

We fix the matching radius at the second internal turning point $R_m = R_2$, thus ensuring the existence of a narrow resonance corresponding to the first eigenvalue in the ho pocket with $Q - v_0 \sim \frac{1}{2}\hbar\omega_0$. One determines β_0 and X_m, and therefore the equilibrium radius R_0. The value of v_0 is given by the first equation (6.4). The internal channel wave functions are given by gaussians with slightly different ho parameters

$$\psi_c^{(int)}(X) = A_c\sqrt{\frac{1}{N}\sqrt{\frac{\beta_c}{\pi}}}e^{-\beta_c X^2/2}. \tag{6.6}$$

The ho parameters and amplitudes are determined by the standard matching con-

ditions

$$\begin{aligned} \beta_c &= -\frac{1}{X_M}\ln'\psi_c^{(ext)}(R_m) \\ A_c &= \psi_c^{(ext)}(R_m)\sqrt{N\sqrt{\frac{\pi}{\beta_c}}e^{\beta_c X_m^2/2}}. \end{aligned} \tag{6.7}$$

The α-particle spectroscopic factor is given by

$$S_\alpha = \int |\Psi(\mathbf{R})|^2 d\mathbf{R} \sim \sum_c A_c^2 \equiv \sum_c S_c. \tag{6.8}$$

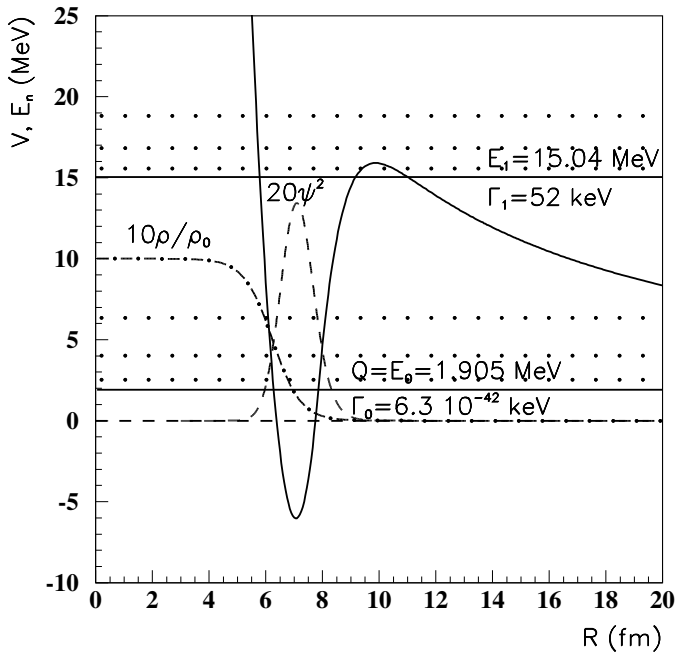

Figure 4: Vibrational resonant states (solid lines) and rotational bands built on them (dotted lines) in the $\alpha - ^{140}$Ce molecular potential. The lower solid line corresponds to the Q-value of the process. The dot-dashed line is 10 times the ratio $\rho(R)/\rho_0$ and the dashed line shows a factor 20 multiplying the gs α-particle probability versus radius [20].

We first analysed the resonant eigenstates in the pocket-like α-core potential. In Fig. 4 we plotted a typical spectrum of resonant states for the transition $^{144}Nd \rightarrow ^{140}$

$Ce + \alpha$ [21]. The first resonant zero node state has the eigenvalue E_0 corresponding to the Q-value, drawn by the lower solid line. Lower solid and dotted lines are eigenstates in the parent nucleus with $J_P = 0^+$, described by coupling the low-lying eigenstates of the daughter nucleus with α-particle states $[L \otimes L]_0$ in Eq. (5.4).

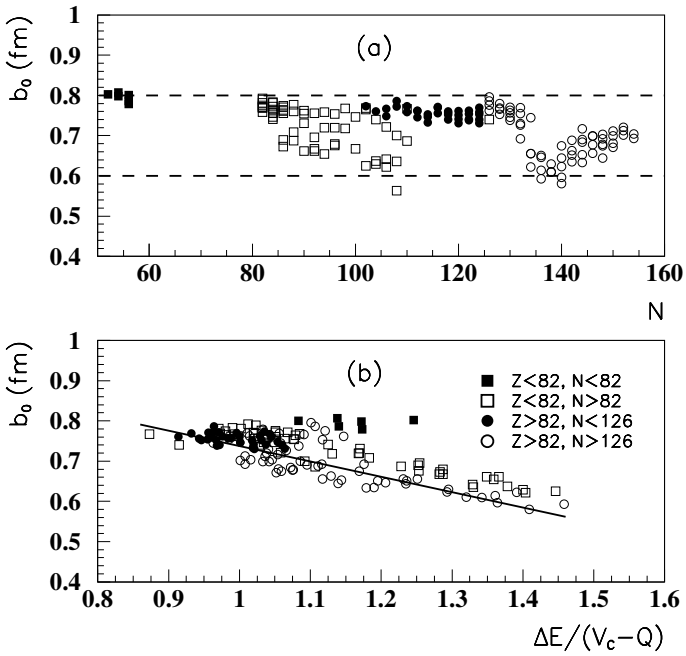

Figure 5: Monopole ho length parameter versus neutron number of the daughter nucleus (a) and versus the ratio between the energy difference of vibrational levels and fragmentation potential (b) for even-even emitters [20]. The symbols denote different regions of the nuclear chart, divided by magic numbers. The regression line in panel (b) fits the data, excepting the first region (dark squares).

We considered experimental energies of the daughter nucleus in the coupled system of equations (5.9), (5.10). A systematic analysis of their B(E2) values is given in Ref. [19]. In Ref. [22], we have shown that for ^{212}Po the low-lying 0^+ α-like resonances (except gs) have small spectroscopic factors and they can be experimentally detected only above 6 MeV. We expect a similar behavior for low lying monopole resonances, plotted by dotted lines in Fig. 4. Thus, they cannot be detected experimentally and the 0^+ states observed around 2 MeV in ^{144}Nd have a different nature.

The upper solid line denotes the next eigenvalue E_1 of the first one-node excited

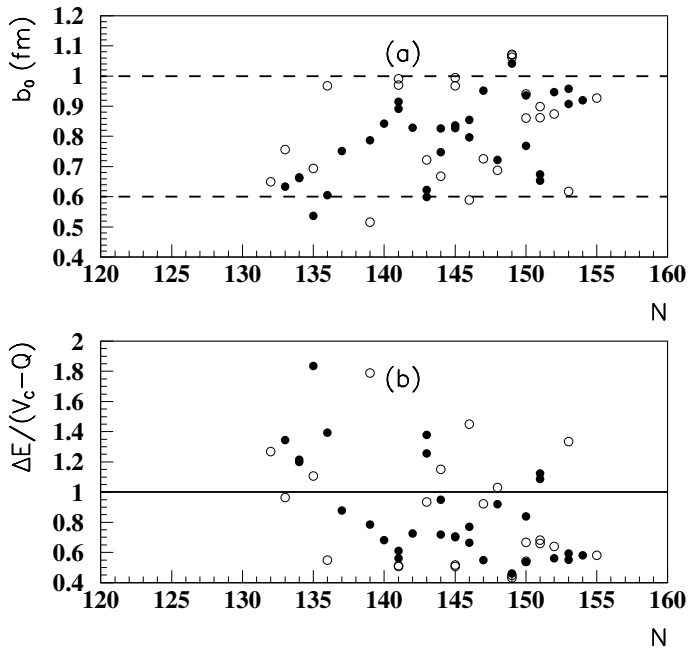

Figure 6: Monopole ho length parameter (a) and the ratio between the energy difference of vibrational levels and fragmentation potential versus neutron number of the daughter nucleus (b) for odd-mass emitters.

vibrational state and the dotted lines above it belong to the excited monopole band with $J_P = 0^+$. The decay width Γ_0 in Fig. 4 is given by the barrier penetration $\Gamma_{pen} = 5\ 10^{-41}$ keV, multiplied with the spectroscopic factor $S_\alpha = 0.125$. It reproduces the input experimental value $\Gamma_{exp} = 6.3\ 10^{-42}$ keV. Moreover, our numerical estimate gives a ratio between errors $\delta\Gamma_1/\delta E_1$=0.16.

The energy difference $\Delta E = E_1 - E_0$ determines the ho parameter of the molecular potential. We plotted the wave function multiplied by 20 with a dashed line, and with a dot-dashed line the ratio between the nuclear and equilibrium density multiplied by 10

$$\frac{\rho(R)}{\rho_0} = \frac{1}{1 + exp[(R - R_n)/a]}, \tag{6.9}$$

by considering a standard diffusivity $a = 0.5$ fm and nuclear radius $R_n = 1.2\ A^{1/3}$. These values are close to the systematics of Ref. [23] based on electron scattering data. Notice that the Mott phase transition point between the nucleonic and α-

clustering phases corresponds to 10% of the equilibrium density in infinite nuclear matter [8] and 20% for ^{212}Po, as seen in Fig. 5 of Ref. [24]. Therefore our calculation confirms that the maximal value of the wave function corresponds to a radius larger than the phase transition point.

As we mentioned before, the rotational quasimolecular band is connected to the ALAS phenomenon. In Ref. [25] it was pointed out that the experimental evidence of this effect was found for a lighter configuration with $Z = 40$, namely $\alpha+^{90}$Zr. Anyway, one sees from Refs. [26, 27] that for the configuration analysed above, $\alpha + Ce$ with $Z = 58$, the ALAS phenomenon disappears close to the Coulomb barrier $V_C \sim 16$ MeV, due to the fact that exchage effects diminish for $Z > 50$.

In Fig. 5 (a), we plotted the ho length parameter b_0 of the gs channel (L=0) as a function of the neutron number in the daughter nucleus for 162 even-even emitters. Notice that $b_0 \in [0.6, 0.8]$ fm, i.e. the ratio to the standard α-particle length parameter $b_\alpha = 1.19$ fm belongs to the interval $b_0/b_\alpha \in [0.5, 0.7]$. In panel (b) is given the length parameter versus the ratio between the energy difference of vibrational levels $\Delta E = E_1 - E_0$ and the fragmentation potential $V_{frag} = V_C(R_{max}) - Q$. Notice that $V_{frag} \in [10, 17]$ MeV. Except for the first region, $Z \sim N \sim 50$ of "superallowed" α-transitions [28], these quantities are linearly correlated. For those nuclei with $b_0 > 0.75$ fm, the rotational band built on the first excited state lies close to the Coulomb barrier $\Delta E/V_{frag} \sim 1$ and therefore it can be detected as a structure of peaks in the energy dependent cross section. The regression line in Fig. 5 (b), fiting the data excepting the first region (dark squares), has a mean error $\langle \delta b_0 \rangle = 0.03$ fm.

The fine structure of odd-mass emitters was measured for $Z \in [87, 100]$. In Fig. 6 we show plots similar to Fig. 5 for odd-mass emitters. Here, one obtains $b_0 \in [0.6, 1] fm$. $\Delta E/V_{frag} \in [0.4, 2]$. Additionally, the $L = 1$ angular momentum of the emitted α-particle is allowed. Thus, the lower and upper vibrational eigenstates in the pocket-like potential of Fig. 4 can be connected by a dipole operator $D \sim X = R - R_0$ of the α-particle center of mass. Therefore, the second vibrational state can be detected in the excitation function of an incident γ beam. Such beams are produced at operating γ-beam facilities, and will be provided in the future at the ELI-NP facility [29].

In Fig. 7 we plotted the spectroscopic factor versus the neutron number of the daughter nucleus. Let us stress on large values above the magic numbers $Z = 50,\ 82$ and $N = 82,\ 126$, where α-molecules are born with significant probabilities [19] and the best candidates for experimental detection have $\Delta E/V_{frag} \sim 1$.

7 Resonances in the α-decay fine structure

Transitions to excited states are a sensitive tool to probe nuclear structure details and to evidence α-clustering on the nuclear surface.

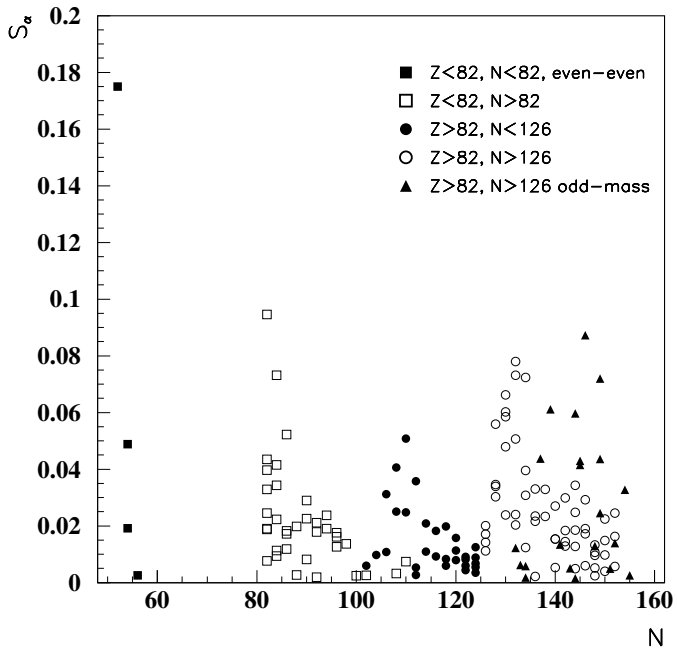

Figure 7: Spectroscopic factor versus neutron number of the daughter nucleus for even-even emitters. The symbols denote different regions of the nuclear chart divided by magic numbers [20].

7.1 Coherent State Model

In Ref. [19] a systematic description of electromagnetic and α-transitions of even-even nuclei was performed in terms of the Coherent State Model (CSM) proposed bty Ref. [30]. This is a tool describing in a unified way the spectra of vibrational, transitional and rotational nuclei. It treats surface vibrations of deformed nuclei by using an exponential superposition of boson operators. The model was later developed for the description of low-lying as well as high spin states in nuclei, including isospin degrees of freedom (for a review, see Ref. [31]).

The wave function of an axially deformed even-even nucleus in the intrinsic system of coordinates is given by a coherent superposition of quadrupole boson operators $b_{2\mu}$ with $\mu = 0$ acting on the vacuum state

$$|\psi_g\rangle = e^{d\left(b^\dagger_{20} - b_{20}\right)}|0\rangle \ , \tag{7.1}$$

in terms of the deformation parameter proportional to the static quadrupole defor-

mation

$$d = \kappa\beta_2 \ . \tag{7.2}$$

Physical states which define the ground band are obtained by projecting out the angular momentum

$$|\varphi_J^{(g)}\rangle = \mathcal{N}_J^{(g)} \widehat{P}_{M0}^J |\psi_g\rangle \ , \tag{7.3}$$

in terms of the projection operator

$$\widehat{P}_{MK}^J = \sqrt{\frac{2J+1}{8\pi^2}} \int \mathrm{d}\omega D_{MK}^J(\omega) \widehat{R}(\omega), \tag{7.4}$$

where $D_{MK}^J(\omega)$ is a Wigner function and $\widehat{R}(\omega)$ is a rotation operator, parametrized by the Euler angles ω. The simplest estimate of the ground band energy spectrum is given by

$$E_J(d) \ = \ A_1 \left[\langle \varphi_J^{(g)} | \widehat{N} | \varphi_J^{(g)} \rangle - \langle \varphi_0^{(g)} | \widehat{N} | \varphi_0^{(g)} \rangle \right] \ , \tag{7.5}$$

where $\widehat{N}$ is the operator for the number of bosons. Notice that for small values of d, the energy spectrum has a vibrational character $E_J \sim A_1 J$, while for large values it has a rotational shape $E_J \sim A_1 J(J+1)$ [30].

7.2 Coupled channels description of α-transitions in even-even nuclei

We apply here the coupled channels framework previously discussed, by considering that the daughter wave function is described by the CSM. The wave function of the α-daughter system has the total spin of the initial ground state (i.e. zero)

$$\begin{aligned} \Psi(b_2, \mathbf{R}) \ &= \ \sum_J \frac{f_J(R)}{R} \mathcal{Z}_J(b_2, \Omega) \\ \mathcal{Z}_J(b_2, \Omega) \ &\equiv \ \left[\varphi_J^{(g)} \otimes Y_J(\Omega) \right]_0 \ . \end{aligned} \tag{7.6}$$

Here, $\varphi_J^{(g)}$ is the J-th eigenstate (7.3) of the CSM Hamiltonian $H_D(b_2)$ in terms of the quadrupole boson b_2 describing the dynamics of the daughter nucleus and $\mathbf{R} \equiv (R, \Omega)$ denotes the distance between the centers of the two fragments. The α-daughter dynamics is described by the stationary Schrödinger equation

$$H\Psi(b_2, \mathbf{R}) = E\Psi(b_2, \mathbf{R}) \ . \tag{7.7}$$

The Hamiltonian describing α-decay is written

$$H = -\frac{\hbar^2}{2\mu} \nabla_R^2 + H_D(b_2) + V(b_2, \mathbf{R}) \tag{7.8}$$

in terms of the reduced mass of the dinuclear system μ. We estimate the interaction between nuclei as a sum of two terms

$$V(b_2, \mathbf{R}) = V_0(R) + V_2(b_2, \mathbf{R}) \ , \tag{7.9}$$

where the monopole part of the interaction is given by the same ansatz as in Ref. [32], i.e.

$$\begin{aligned} V_0(R) &= v_a \overline{V}_0(R) \ , \quad R > R_m \\ &= c(R - R_{min})^2 - v_0 \ , \quad R \leq R_m \ . \end{aligned} \tag{7.10}$$

Here, $\overline{V}_0$ is the nuclear plus Coulomb interaction, estimated by using the double folding procedure within the M3Y particle-particle interaction with Reid soft core parametrisation [11, 12, 13]. The value $v_a = 1$ corresponds to a "pure" α-cluster model. By considering $v_a < 1$ one assumes an α-cluster probability less than unity, necessary to reproduce the experimental half life. The second line is the repulsive core simulating the Pauli effect and fixing the energy of the first resonant state to the experimental Q-value.

We applied the procedure of Ref. [32] to determine the matching radius R_m and the coordinate R_{min}, corresponding to the minimal value, by using the equality between the external attractive and internal repulsion, together with their derivatives (see Eqs. (32) of this reference). Thus, the above interaction is continuous and it depends upon only one independent parameter, due to the fact that the repulsive strength c is inversely proportional with respect to the potential depth v_0 [32].

The $\lambda = 2$ term is given by the quadrupole-quadrupole (QQ) interaction

$$V_2(b_2, \mathbf{R}) = -C_0(R - R_{min}) \frac{dV_0(R)}{dR} \widehat{2} \left[Q_2 \otimes Y_2(\Omega) \right]_0 \ . \tag{7.11}$$

By using the orthonormality of angular functions entering the superposition (7.6) one obtains in a standard way the coupled system of differential equations for radial components [17]

$$\frac{d^2 f_J(R)}{d\rho_J^2} = \sum_{J'} A_{JJ'}(R) f_{J'}(R) \ , \tag{7.12}$$

where the coupling matrix is given by

$$A_{JJ'}(R) = \left[\frac{J(J+1)}{\rho_J^2} + \frac{V_0(R)}{E - E_J} - 1 \right] \delta_{JJ'} + \frac{1}{E - E_J} \langle \mathcal{Z}_J | V_2(b_2, \mathbf{R}) | \mathcal{Z}_{J'} \rangle \ , \tag{7.13}$$

in terms of the reduced radius

$$\rho_J = \kappa_J R \ , \quad \kappa_J = \sqrt{\frac{2\mu(E - E_J)}{\hbar^2}} \ . \tag{7.14}$$

The matrix element of the particle-core coupling entering Eq. (7.13) is given in Ref. [30] and it is proportional to the reduced matrix element defining electromagnetic transitions, but with a different anaharmonic parameter

$$\begin{aligned}\langle \mathcal{Z}_J|V_2(b_2,\mathbf{R}|\mathcal{Z}_{J'}\rangle &= -C_0(R-R_{min})\frac{dV_0(R)}{dR}\frac{1}{\widehat{2}\widehat{J}\widehat{J'}}\langle\varphi_J^{(g)}||Q_2||\varphi_{J'}^{(g)}\rangle\langle Y_J||Y_2||Y_{J'}\rangle \\ &= -C(d)\,(R-R_{min})\,\frac{dV_0(R)}{dR}\frac{d}{\sqrt{4\pi}}\frac{\widehat{J}}{\widehat{J'}}\langle J0;20|J'0\rangle^2 \\ &\times \left(\frac{\widehat{J'}\mathcal{N}_{J'}^{(g)}}{\widehat{J}\mathcal{N}_J^{(g)}}+\frac{\widehat{J}\mathcal{N}_J^{(g)}}{\widehat{J'}\mathcal{N}_{J'}^{(g)}}\right)\ , \end{aligned} \tag{7.15}$$

where we defined the effective α-daughter coupling strength

$$C(d)=C_0\left(1-\sqrt{\frac{2}{7}}a_\alpha d\right)\ . \tag{7.16}$$

In order to solve the system of quations (7.12) let us first define the internal and external fundamental solutions satisfying the following boundary conditions:

$$\begin{aligned}\mathcal{R}_{JI}(R) &\overset{R\to R_0}{\longrightarrow} \delta_{JI}\varepsilon_J\ , \\ \mathcal{H}_{JI}^{(+)}(R)\equiv\mathcal{G}_{JI}(R)+i\mathcal{F}_{JI}(R) &\overset{R\to\infty}{\longrightarrow} \delta_{JI}H_J^{(+)}(\kappa_J R)\equiv\delta_{JI}\left[G_J(\kappa_J R)+iF_J(\kappa_J R)\right]\ . \end{aligned} \tag{7.17}$$

Here, R_0 is a radius inside the internal repulsive potential and ε_J are arbitrary small numbers. The index J labels the component and I solution, $G_J(\kappa_J R)$, $F_J(\kappa_J R)$ are the irregular and regular spherical Coulomb wave functions depending on the momentum κ_J in the channel J.

Each component of the solution is built as a superposition of N independent fundamental solutions. We impose the matching conditions at some radius R_1 inside the barrier

$$\begin{aligned} f_J(R_1) &= \sum_I \mathcal{R}_{JI}(R_1)M_I=\sum_I \mathcal{H}_{JI}^{(+)}(R_1)N_I \\ \frac{df_J(R_1)}{dR} &= \sum_I \frac{d\mathcal{R}_{JI}(R_1)}{dR}M_I=\sum_I \frac{d\mathcal{H}_{JI}^{(+)}(R_1)}{dR}N_I\ , \end{aligned} \tag{7.18}$$

where N_I are called scattering amplitudes. The conditions (7.18) give the following secular equation

$$\begin{aligned} &\begin{vmatrix} \mathcal{R}(R_1) & \mathcal{H}^{(+)}(R_1) \\ \frac{d\mathcal{R}(R_1)}{dR} & \frac{d\mathcal{H}^{(+)}(R_1)}{dR}\end{vmatrix} \\ \approx\ &\begin{vmatrix} \mathcal{R}(R_1) & \mathcal{G}(R_1) \\ \frac{d\mathcal{R}(R_1)}{dR} & \frac{d\mathcal{G}(R_1)}{dR}\end{vmatrix}=0\ . \end{aligned} \tag{7.19}$$

The first condition is fulfilled for complex energies, determining the resonant states. They practically coincide with the real scattering resonant states, due to the fact that the imaginary parts of energies are much smaller than the corresponding real parts, corresponding to vanishing regular Coulomb functions F_J inside the barrier. The roots of the equation (7.19) do not depend upon the matching radius R_1, because both internal and external solutions satisfy the same Schrödinger equation. The unknown coefficients M_I, N_I are determined from the normalisation of the wave function in the internal region

$$\sum_J \int_{R_0}^{R_3} |f_J(R)|^2 dR = 1 \ , \tag{7.20}$$

where R_3 is the external turning point. All known half-lives in α emission are much larger that the characteristic nuclear time $T_{min} \approx 10^{-6}\ s >> T_N \approx 10^{-22}\ s$. Thus, any α-decaying state practically behaves like a bound state, having an exponential decrease versus radius inside the barrier.

¿From the continuity equation one obtains the total decay width as a sum of partial widths

$$\begin{aligned} \Gamma &= \sum_J \Gamma_J = \sum_J \hbar v_J \lim_{R\to\infty} |f_J(R)|^2 \\ &= \sum_J \hbar v_J |\mathcal{N}_J|^2 \ , \end{aligned} \tag{7.21}$$

where v_J is the center of mass velocity at infinity in the channel J, i.e.

$$v_J = \frac{\hbar \kappa_J}{\mu} \ . \tag{7.22}$$

We used the CSM deformation parameter d, given by analyzing low-lying energy levels, in order to determine the α-decay fine structure, defined by the logarithm of the ratio between decay widths to ground and J^+ states

$$I_J \equiv \log_{10} \frac{\Gamma_0}{\Gamma_J} \ , \tag{7.23}$$

where partial widths are given by Eq. (7.21). We call this quantity the intensity of the α-decay to the J-th state. In our calculations we considered $v_a = 1$ and fixed the value of the repulsive strength $c = 50$ MeV, as in Ref. [33], thus changing the only remaining free parameter v_0 in order to reproduce the Q-value for each α-decay.

By using the effective α-daughter coupling strength $C(d)$, we reproduced the available experimental quadrupole intensities I_2. In Fig. 8 (a) we plotted the values of this strength as a function of the deformation d. Thus, we indeed obtained the linear dependence of the α-daughter QQ coupling strength with a negative slope,

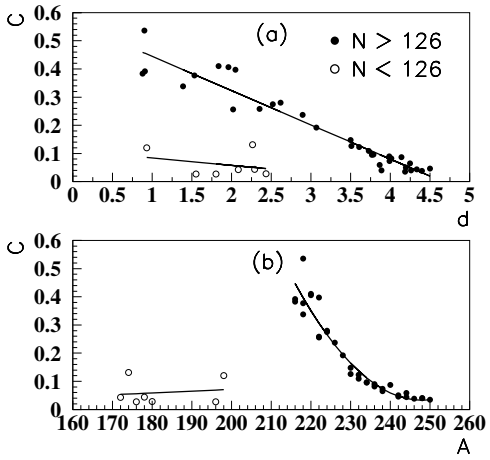

Figure 8: (a) α-daughter QQ coupling strength C defined by Eq. (7.16) versus the deformation parameter d. (b) Same as in (a), but for the mass number A [18].

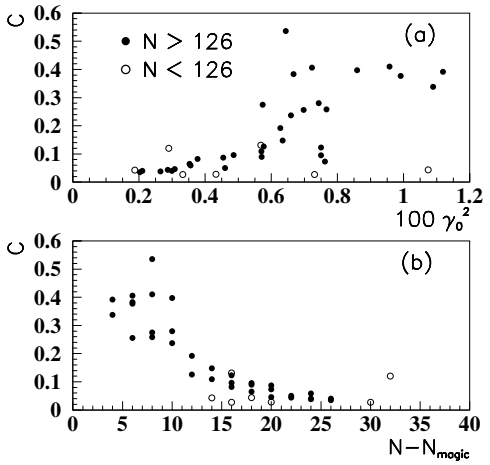

Figure 9: (a) α-daughter QQ coupling strength C defined by Eq. (7.16) versus the α-particle reduced width. (b) Same as in (a), but versus $N - N_{magic}$, where $N_{magic} = 126$ for $N > 126$, $N_{magic} = 82$ for $N < 126$ [18].

predicted by Eq. (7.16). Notice that for the region $N < 126$ the values belong a narrow interval of small values $C \in [0.05, 0.1]$.

It turns out that the QQ strength is also related to the mass number A. In Fig. 8 (b) we give the dependence of this strength versus A. The α-daughter QQ coupling is stronger for nuclei above ^{208}Pb, where $C \approx 0.5$, i.e. in the region where the α-clustering is larger [15]. It decreases by one order of magnitude around the mass region $A = 240$. By crossing the shell closure to the region $N < 126$ it jumps by one order of magnitude, up to the value $C \approx 0.05$. Let us stress here that for $N > 126$ this behaviour is similar to the dependence of the reduced width (called α-particle probability) for transitions connecting ground states with J=0. Indeed, it turns out that the α-daughter strength is proportional to the α-particle probability, with different slopes for $N > 126$ (dark circles) and $N < 126$ (open symbols), as we can see in Fig. 9 (a). Notice that the dependence versus the number of neutrons above the closed shell N_{magic} is common for both regions, as we can see in Fig. 9 (b). This proves the α-like resonant quasimolecular picture of an α-cluster moving around a doubly magic core. Several α-clusters are rapidly "disolved" due to the Pauli principle.

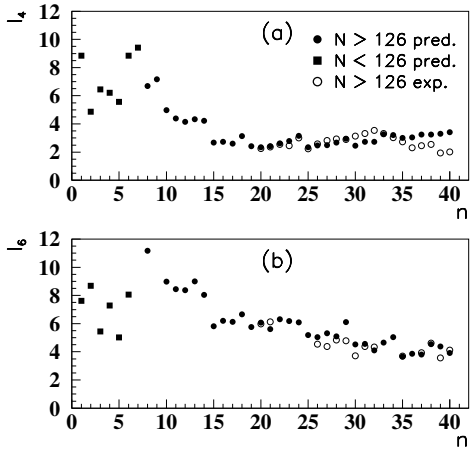

Figure 10: (a) Predicted intensity I_4, by using the coupling strength $C(d)$ reproducing the corresponding value I_2, versus the index n in the first column of the Table I. (b) Same as in (a), but for I_6 [18].

We used these values of the α-daughter strength C(d) reproducing I_2 values in order to predict the intensities I_4 and I_6. They are plotted in Fig. 10 by dark symbols versus the index n. These values reproduce the available experimental data, plotted by open circles, with a reasonable accuracy. This proves that this relatively simple model is able to simultaneously describe all available experimental α-decay intensities to excited states within a range of four orders of magnitude.

8 α-like collective resonances

We will investigate the possibility of a new collective motion performed by α-clusters with respect to the remaining core [34]. We will analyze the collective modes generated by the relative motion of protons, neutrons and α-clusters, by generalizing the procedure proposed by D. Brink to describe giant resonance in Ref. [35] and used in Ref. [36] for the pygmy resonance. Let us consider four subsystems: Z_c core protons, N_c core neutron, N_e excess neutrons with the same mass m and Q α-clusters with effective mass m_α, moving in a ho mean field

$$\begin{aligned} H &= \sum_{i=1}^{Z_c} \frac{\mathbf{P}_{p,i}^2}{2m} + \sum_{i=1}^{N_c} \frac{\mathbf{P}_{n,i}^2}{2m} + \sum_{i=1}^{N_e} \frac{\mathbf{P}_{e,i}^2}{2m} + \sum_{i=1}^{Q} \frac{\mathbf{P}_{\alpha,i}^2}{2m_\alpha} \\ &+ \frac{m\omega_0^2}{2} \sum_{i=1}^{Z_c} \mathbf{r}_{p,i}^2 + \frac{m\omega_0^2}{2} \sum_{i=1}^{N_c} \mathbf{r}_{n,i}^2 + \frac{m\omega_0^2}{2} \sum_{i=1}^{N_e} \mathbf{r}_{e,i}^2 + \frac{m_\alpha\omega_0^2}{2} \sum_{i=1}^{Q} \mathbf{r}_{\alpha,i}^2 \ . \end{aligned} \tag{8.24}$$

The frequency ω_0 is obtained from the requirement to reproduce the mean square radius of a sphere of nuclear radius, its value being $\hbar\omega_0 = 41\ A^{-1/3} MeV$. This Hamiltonian may be arranged in the following form

$$\begin{aligned} H &= \frac{\mathbf{P}_p^2}{2mZ_c} + \frac{\mathbf{P}_n^2}{2mN_c} + \frac{\mathbf{P}_e^2}{2mN_e} + \frac{\mathbf{P}_\alpha^2}{2m_\alpha Q} \\ &+ \frac{m\omega_0^2}{2} Z_c \mathbf{R}_p^2 + \frac{m\omega_0^2}{2} N_c \mathbf{R}_n^2 + \frac{m\omega_0^2}{2} N_e \mathbf{R}_e^2 + \frac{m_\alpha\omega_0^2}{2} Q \mathbf{R}_\alpha^2 \\ &+ \text{internal part} \ . \end{aligned} \tag{8.25}$$

Let us define the core, core+excess neutrons, effective α-cluster and total mass numbers

$$A_c = Z_c + N_c \ , \quad A_0 = A_c + N_e \ , \quad A_\alpha = Q \cdot \frac{m_\alpha}{m} \ , \quad A = A_0 + A_\alpha \ . \tag{8.26}$$

The collective part of the Hamiltonian becomes

$$H = \frac{1}{2m} \left(\frac{\mathbf{P}_p^2}{Z_c} + \frac{\mathbf{P}_n^2}{N_c} + \frac{\mathbf{P}_e^2}{N_e} + \frac{\mathbf{P}_\alpha^2}{A_\alpha} \right) + \frac{m\omega_0^2}{2} \left(Z_c \mathbf{R}_p^2 + N_c \mathbf{R}_n^2 + N_e \mathbf{R}_e^2 + A_\alpha \mathbf{R}_\alpha^2 \right) \tag{8.27}$$

Let us separate the center of mass (cm) motion of the nucleus from the other modes of oscillation. The cm position is

$$\mathbf{R}_{CM} = \frac{Z_c \mathbf{R}_p + N_c \mathbf{R}_n + N_e \mathbf{R}_e + A_\alpha \mathbf{R}_\alpha}{Z_c + N_c + N_e + A_\alpha} \ , \tag{8.28}$$

while the coordinate describing the oscillation of the core protons against the core neutrons is

$$\mathbf{X}_C = \mathbf{R}_p - \mathbf{R}_n \ . \tag{8.29}$$

The motion of the core against the excess neutrons is given by

$$\mathbf{Y} = \mathbf{R}_{CM,core} - \mathbf{R}_e = \frac{Z_c\mathbf{R}_p + N_c\mathbf{R}_n}{Z_c + N_c + N_e} - \mathbf{R}_e \ . \tag{8.30}$$

We now introduce the coordinate which gives the motion of the system core+excess neutrons against the clusters

$$\mathbf{Y}_\alpha = \mathbf{R}_{CM,core+exc} - \mathbf{R}_\alpha = \frac{Z_c\mathbf{R}_p + N_c\mathbf{R}_n + N_e\mathbf{R}_e}{Z_c + N_c + N_e} - \mathbf{R}_e \ . \tag{8.31}$$

The Hamiltonian acquires the diagonal form

$$H = \sum_{K=CM,C,y,\alpha} \left(\frac{\mathbf{P}_K^2}{2M_K} + \frac{M_k\omega_0^2}{2}\mathbf{X}_K^2 \right) \ , \tag{8.32}$$

where the effective masses corresponding to each mode are given by

$$M_{CM} = mA \ , \quad M_C = m\frac{N_cZ_c}{A_c} \ , \quad M_y = m\frac{N_eA_c}{A_0} \ , \quad M_\alpha = m\frac{A_\alpha A_0}{A} \ . \tag{8.33}$$

Let us now introduce the dipole operator

$$\begin{aligned} \mathbf{D} &= e\sum_{i=1}^{Z_c}(\mathbf{r}_{p,i} - \mathbf{R}_{CM}) + e_\alpha\sum_{i=1}^{Q}(\mathbf{r}_{\alpha,i} - \mathbf{R}_{CM}) \\ &= eZ_c(\mathbf{R}_p - \mathbf{R}_{CM}) + e_\alpha Q(\mathbf{R}_\alpha - \mathbf{R}_{CM}) \ . \end{aligned} \tag{8.34}$$

We use the notations for the ratios of the effective charge and mass of the cluster to those of the nucleon $\epsilon = e_\alpha/e$, $\mu = m_\alpha/m$. By adjusting the values of these parameters, the effects of clusters of any size may be evaluated. However, the spectroscopic factors for heavy clusters are much smaller than in the α-cluster case, making such oscillations unobservable [37].

The dipole operator is divided into terms belonging to (1) the core-proton against core-neutron oscillation, (2) the core against extra-neutron oscillation and (3) the oscillation of the alpha particles against all other constituents, i.e. $\mathbf{D} = \mathbf{D}_C + \mathbf{D}_y + \mathbf{D}_\alpha$, where

$$\begin{aligned} \mathbf{D}_C &= \frac{Z_cN_c}{A_c}\mathbf{X}_C \equiv d_C\mathbf{X}_C \ , \\ \mathbf{D}_y &= \frac{Z_cN_e}{A_0}\mathbf{Y} \equiv d_y\mathbf{Y} \ , \\ \mathbf{D}_\alpha &= \frac{A_\alpha}{A}\left(Z_c - \frac{\epsilon}{\mu}A_0\right)\mathbf{Y}_\alpha \equiv d_\alpha\mathbf{Y}_\alpha \ . \end{aligned} \tag{8.35}$$

The residual dipole-dipole interaction to the Hamiltonian of Eq. (8.32) is necessary in order to reproduce the experimental values of the GDR frequency. Previous

studies investigated the coupling of the $\mathbf{X}_C$ and $\mathbf{Y}$ modes by the dipole-dipole interaction in schematic models based on the on the Tamm-Dancoff and random phase approximations [38] and within the ho shell model [39]. In the present work, we generalize the latter by including the mode corresponding to the α type resonance $\mathbf{Y}_\alpha$

$$H_{int} = \frac{1}{2} \sum_{K,L=C,y,\alpha} \chi_{KL}\, \mathbf{D}_K \cdot \mathbf{D}_L = \frac{1}{2} \sum_{K,L=C,y,\alpha} \chi_{KL}\, d_K d_L\, \mathbf{X}_K \cdot \mathbf{X}_L\ . \qquad (8.36)$$

The Hamiltonian H_{tot} of our model is thus obtained by taking into account Eqs. (8.32) and (8.36), $H_{tot} = H + H_{int}$. The normal modes are obtained as superpositions of the individual modes C, y, α, after the diagonalization procedure. Each normal K mode has a dominant contribution from the original C, y, or α modes, and the total Hamiltonian becomes $H_{tot} = \sum_{K=1,2,3} H_K$.

The total dipole absorption cross section of a given normal mode K, giving the fraction of the energy weighted sum rule (EWSR) exhausted by the mode, may be estimated by using the Thomas-Reiche-Kuhn sum rule (see standard textbooks, e.g. Appendix B of [40], Section 5.6 of [41])

$$\sigma_K = \frac{4\pi^2 e^2}{\hbar c} \sum_f (E_f - E_0)\, |\langle f|D_K|0\rangle|^2 = \frac{4\pi^2 e^2}{\hbar c} \frac{1}{2} \langle 0|\, [D_K, [H_K, D_K]]\, |0\rangle \qquad (8.37)$$

where D_K is the dipole operator corresponding to the mode K. In our schematic approach we consider only the dipole-dipole residual interaction, but it is important to mention that other components of the nucleon-nucleon interaction, especially the tensor force, are relevant for the full understanding of the dipole strength function and the energy-weighted sum rule.

We simulated the nuclear mean field by a schematic ho well neglecting the spin-orbit interaction. In cluster models, where composite objects are formed from nucleons lying on the mean field levels, the Pauli principle may be taken into account by restricting the values of the radial and angular momentum quantum numbers of the cluster component. The antisymmetrisation effects are reproduced if the number of cluster excitation quanta G = 2N + L is restricted to values greater than the sum over the single particle quantum number of the cluster nucleons that are excluded from below the Fermi energy, $\sum_c (2n_c + l_c)$. This approach, known as the Wildermuth rule, is widely used to describe alpha and heavy cluster formation in a potential well, by using an effective value of the quantum number G in order to satisfy the Bohr-Sommerfeld rule entering the quantization condition [42]. In our case, the nucleons and clusters move in the same ho potential. The dipolar operator promotes the clusters on a higher level, changing the angular momentum/parity by one unit. Thus, all nucleons forming the clusters are automatically promoted above the Fermi sea, satisfying the Wildermuth rule. In a microscopic picture, they are localizated on the nuclear surface, and the cluster state may be thought of as an

additional Gaussian attractive component on the surface region of the mean field [28, 43]. The overlap of the cluster state with the internal core functions is negligible, as a manifestation of the Pauli principle. In our model, the only restriction is connected to the strength of the dipole-dipole interaction, which should have a definite value. Obviously, for a realistic Woods-Saxon mean field the excited resonance is found in the continuum and practically any value of the dipole strength is allowed.

In order to analyze the interplay between the usual giant dipole resonance (GDR) and α-like resonance we will first consider the symmetric system with $N = Z$, where the pygmy resonance induced by neutrons in excess disappears. The fraction of the EWSR exhausted by the α-like mode may be estimated from Eq. (8.35), as follows

$$f_\alpha = \frac{\left(1-\frac{2\epsilon}{\mu}\right)^2}{\left(1-\frac{2\epsilon}{\mu}\right)^2 + 1 + \frac{A_c}{\mu Q}} \ , \tag{8.38}$$

and is seen to be independent of the alpha and GDR self couplings.

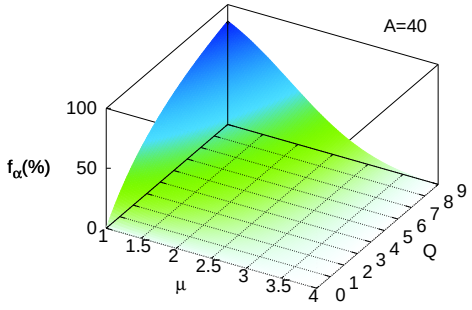

Figure 11: α-mode EWSR fraction vs effective cluster mass and number of clusters [34].

The alpha clusters do not exist with a probability of unity inside the nucleus. This fact is quantitatively described by the cluster spectroscopic factor, estimated as the spatial integral of the α-particle formation amplitude squared. It has the maximal value $S_\alpha < 0.01$ for lightest α-emitters above ^{100}Sn [28]. For instance, a spectroscopic factor $S_\alpha = 0.01$ corresponds to the case where for 1/100 of the time one has a real alpha-particle with four nucleonic masses and 99/100 of the time one has free nucleons. We simulate this probability by an effective alpha-particle mass. Thus, we define the effective mass by the probabilistic average

$$m_\alpha = p_\alpha m_{\alpha,0} + (1-p_\alpha) m_n \ , \tag{8.39}$$

where m_n is the nucleon mass, $m_{\alpha,0} = 4m_n$ is the bare α-cluster mass, and $p_\alpha = S_\alpha$ is the probability of formation of the α-cluster.

Therefore one has $\mu < 1.03$ and the smallest value of the α-mode EWSR fraction is $f_\alpha \sim 10\%$ above the the doubly magic nucleus ^{100}Sn. An interesting conclusion is that for light systems, where $\mu \sim 4$, this fraction has lower values. This behaviour is compensated by the increase of α-cluster number, as can be seen in Fig. 11, where we plotted f_α versus the number of clusters for various effective masses. This quantity increases versus the number of clusters but decreases by increasing the spectroscopic factor (effective mass).

Let us consider the influence of the pygmy resonance induced by the excess neutrons. We will work within the zero inter-mode coupling case. By allowing the presence of excess neutrons, the α-fraction of the EWSR becomes

$$f_\alpha = \frac{\left[1 - \frac{2\epsilon}{\mu}\left(1 + \frac{N_e}{A_c}\right)\right]^2}{\left(1 + \frac{N_e}{A_c}\right)\left[\left(1 - \frac{2\epsilon}{\mu}\right)^2 + 1 + \frac{A_c}{\mu Q} + \left(\frac{2\epsilon}{\mu}\right)^2 \frac{N_e}{A_c}\right]} \ . \tag{8.40}$$

The EWSR exhausted by the pygmy mode may be computed in a similar manner. The ratio of α and pygmy modes' exhausted EWSR is given by:

$$\frac{f_\alpha}{f_y} = \frac{\mu Q}{A}\left[\left(1 - \frac{2\epsilon}{\mu}\right)\sqrt{\frac{A_c}{N_e}} - \frac{2\epsilon}{\mu}\sqrt{\frac{N_e}{A_c}}\right]^2 \ . \tag{8.41}$$

We plot the dependence of this ratio as a function of the effective α-mass and the excess neutrons in Figs. 12 and 13.

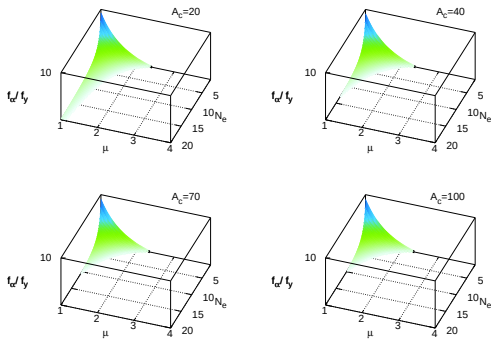

Figure 12: Ratio between α and pygmy EWSR fractions vs excess neutrons and effective α mass (Q=1). Only values larger than unity are shown [34].

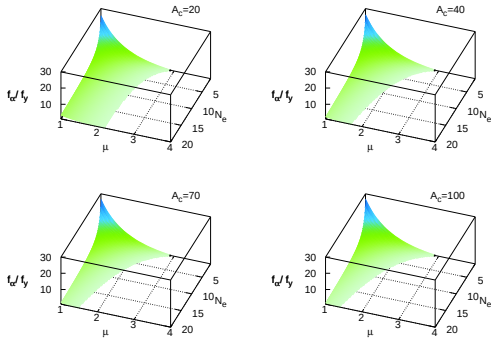

Figure 13: Ratio between α and pygmy EWSR fractions vs excess neutrons and effective α mass (Q=3). Only values larger than unity are shown [34].

The frequencies of the GDR, pygmy and α modes may be estimated as follows

$$\begin{aligned}
\omega^2_{GDR} &= \omega^2_0 + \frac{\chi_c}{m}\frac{A_c}{4} \ , \\
\omega^2_y &= \omega^2_0 + \frac{\chi_y}{m}\frac{A_c}{4}\frac{N_e}{A_c+N_e} \ , \\
\omega^2_\alpha &= \omega^2_0 + \chi_\alpha \frac{A_c}{4m}\frac{\mu Q A_c}{A(A_c+N_e)}\left[1-\frac{2\epsilon}{\mu}\left(1+\frac{N_e}{A_c}\right)\right]^2 \ . \qquad (8.42)
\end{aligned}$$

In particular, in this case of decoupled modes, one obtains

$$\frac{\omega^2_\alpha-\omega^2_0}{\omega^2_y-\omega^2_0} = \frac{\chi_\alpha}{\chi_y}\frac{f_\alpha}{f_y} \ . \qquad (8.43)$$

The α and pygmy frequencies are very close to each other, around 8 MeV above ^{100}Sn. In Fig. 12 we plotted the ratio between α and pygmy EWSR fractions versus the excess of neutrons and effective α mass for the number of quartets Q=1. As expected, this ratio decreases by increasing the number of excess neutrons. As we can see, the unexpected decreasing behaviour versus the increase of the effective mass (i.e. spectroscopic factor) is similar to the previous N=Z case. In Fig. 13 we plotted the same dependencies, but for Q=3 α-clusters. One sees that the results are very close to the previous case.

Let us mention that this model has no theoretical constraints to the existence of α-oscillations. However, as obtained from our analysis, the α-mode fraction of the total EWSR diminishes with an increasing mass number. Thus, we do not expect that superheavy nuclei will have any relevant α-dipolar response.

9 Conclusions

We reviewed the phenomenological model of an α-particle moving in a pocket-like quasimolecular potential, explaining the gross features of the decay data between ground as well as to excited states. We also extended the Brink model to describe the α-cluster dynamics in a similar way to giant resonances, thus evidencing the possibility to detect α-like collective resonances.

References

[1] B. H. Flowers and M. Vujicik, Nucl. Phys. **49**, 586 (1963).

[2] D. M. Brink, *Alpha cluster model*, Proceedings of the International School of Physics Enrico Fermi, Varenna, 1965, Course 36, edited by C. Bloch (Academic, New York, 1966), p. 247.

[3] A. Arima and V. Gillet, Ann. Phys. (NY) **66**, 117 (1971).

[4] K. Wildermuth and Y. C. Tang, *A Unified Theory of the Nucleus* (Academic, New York, 1977).

[5] Y. K. Gambhir, P. Ring, and P. Schuck, Phys. Rev. Lett. **51**, 1235 (1983).

[6] D.S. Delion, G. G. Dussel, and R. J. Liotta, Rom. J. Phys. **47**, 97 (2002).

[7] Y. Funaki, H. Horiuchi, W. von Oertzen, G. Rpke, P. Schuck, A. Tohsaki, and T. Yamada, Phys. Rev. C **80**, 064326 (2009).

[8] G. Röpke, A. Schnell, P. Schuck, and P. Nozieres, Phys. Rev. Lett. **80**, 3177 (1998).

[9] A. Tohsaki, H. Horiuchi, P. Schuck, and G. Rpke, Rev. Mod. Phys. **89**, 011002 (2017).

[10] W. von Oertzen, M. Freer, and Y. Kanada-Enyo, Physics Reports **432** (2006) 43.

[11] G. Bertsch, J. Borysowicz, H. McManus, and W.G. Love, Nucl. Phys. A **284**, 399 (1977).

[12] G.R. Satchler and W.G. Love, Phys. Rep. **55**, 183 (1979).

[13] F. Cârstoiu and R.J. Lombard, Ann. Phys. (N.Y.) **217**, 279 (1992).

[14] Dao T. Khoa, Phys. Rev. C **63**, 034007 (2001).

[15] D. S. Delion, Phys. Rev. **C** 80, 024310 (2009).

[16] V.E. Viola and G.T. Seaborg, J. Inorg. Nucl. Chem. **28**, 741 (1966).

[17] D.S. Delion, *Theory of particle and cluster emission* (Springer-Verlag, Berlin, 2010).

[18] D.S. Delion and A. Dumitrescu, Phys. Rev. C **87**, 044314 (2013).

[19] D.S. Delion and A. Dumitrescu, Atomic Data and Nuclear Data Tables **101** (2015) 1.

[20] D.S. Delion, A. Dumitrescu, and V.V. Baran, Phys. Rev. C **97**, 064303 (2018).

[21] P. Mohr, Phys. Rev. C **61**, 045802 (2000).

[22] D.S. Delion and J. Suhonen, Phys. Rev. C **61**, 024304 (2000).

[23] H. de Vries, C.W. de Jager, and C. de Vries, Atomic Data Nuclear Data Tables **36**, 495536 (1987).

[24] G. Röpke, P. Schuck, Y. Funaki, H. Horiuchi, Zhongzhou Ren, A. Tohsaki, Chang Xu, T. Yamada, and Bo Zhou, Phys. Rev. C **90**, 034304 (2014).

[25] S. Ohkubo, Phys. Rev. Lett. **74**, 2176 (1995).

[26] B.D. Watson, D. Robson, D.D. Tolbert, and R.H. Davis, Phys. Rev. C **4**, 2240 (1971).

[27] P. Mohr, Phys. Rev. C **87**, 035802 (2013).

[28] V.V. Baran and D.S. Delion, Phys. Rev. C **94**, 034319 (2016).

[29] N.V. Zamfir, Eur. Phys. J. Special Topics **223**, 1221 (2014); EPJ Web of Conferences **66**, 11043 (2014).

[30] A.A. Raduta and R.M. Dreizler, Nucl. Phys. A **258**, 109 (1976).

[31] A.A. Raduta, R. Budaca, and Amand Faessler, Ann. Phys. (NY) **327**, 671 (2012).

[32] D.S. Delion, S. Peltonen, and J. Suhonen, Phys. Rev. C **73**, 014315 (2006).

[33] D.S. Delion, S. Peltonen, and J. Suhonen, Phys. Rev. C **78**, 034608 (2008).

[34] V.V. Baran and D.S. Delion, J. Phys. G **45**, 035106 (2018).

[35] D.M. Brink, Nucl. Phys. **4**, 215 (1957).

[36] V. Baran, B. Frecus, B. Colonna. and M. Di Toro, Phys. Rev. C **85**, 051601 (2012).

[37] R. Blendowske and H. Walliser, Phys. Rev. Lett. **61**, 1930 (1998).

[38] V. Baran, D.I. Palade, M. Colonna, M. Di Toro, A. Croitoru, A.I. Nicolin Phys. Rev. C **91**, 054303 (2015).

[39] A. Croitoru, V. Baran, T. Isdraila, M. Colonna, M. Di Toro, M. Marciu, Rom. Journ. Phys. **60**, 748 (2015).

[40] P. Ring, P. Schuck P, *The nuclear many body problem* (Springer-Verlag, New York, 1980).

[41] J.M. Eisenberg and W. Greiner, *Excitation mechanisms of the nucleus* (North-Holland Publishing Company, 1976).

[42] B. Buck, J.C. Johnston, A.C. Merchant, S.M. Perez, Phys. Rev. **52**, 1840 (1995).

[43] D.S. Delion and R.J. Liotta, Phys. Rev. C **87**, 041302 (2013).